# Environmental test of the BGO calorimeter for DArk Matter Particle Explorer *

Yi-Ming Hu(胡一鸣)[1,2,3;1)] Jin Chang(常进)[1,2] Deng-Yi Chen(陈灯意)[1,2] Jian-Hua Guo(郭建华)[1,2]
Yun-Long Zhang(张云龙)[4] Chang-Qing Feng(封常青)[4]

[1] Key Laboratory of Dark Matter and Space Astronomy, CAS 2010DP173032, Nanjing 210008, China
[2] Purple Mountain Observatory, Chinese Academy of Sciences, Nanjing 210008, China
[3] University of Chinese Academy of Sciences, Beijing 100049, China
[4] University of Science and Technology of China, Hefei 230026, China

**Abstract:** DArk Matter Particle Explorer (DAMPE) is the first Chinese astronomical satellite, successfully launched on Dec. 17 2015. As the most important payload of DAMPE, the BGO calorimeter contains 308 bismuth germanate crystals, with 616 photomultiplier tubes, one coupled to each end of every crystal. Environmental tests have been carried out to explore the environmental adaptability of the flight model of the BGO calorimeter. In this work we report the results of the vibration tests. During the vibration tests, no visible damage occurred in the mechanical assembly. After random or sinusoidal vibrations, the change of the first order natural frequency of BGO calorimeter during the modal surveys is less than 5%. The shift ratio of Most Probable Value of MIPs changes in cosmic-ray tests are shown, the mean value of which is about −4%. The comparison of results of cosmic-ray tests before and after the vibration shows no significant change in the performance of the BGO calorimeter. All these results suggest that the calorimeter and its structure have passed through the environment tests successfully.

**Keywords:** detector, dark matter, calorimeter, environmental test

**PACS:** 29.40.Vj **DOI:** 10.1088/1674-1137/40/11/116003

## 1 Introduction

In the standard cosmology model, normal matter, dark matter and dark energy make up about 4.9%, 26.6% and 68.5% respectively of the energy of the current Universe. Though the dark matter is known to be abundant, its nature is largely unknown [1]. It is widely speculated that dark matter particles may annihilate with each other or alternatively decay and then produce stable particle pairs, in particular electrons/positrons and high energy gamma-rays [1–3]. The indirect detection of dark matter in space has attracted wide attention. Many space detectors such as Fermi-LAT, PAMELA and AMS-02 have been launched to probe this largely uncharted territory [4–6]. Tentative evidence includes the electron/positron excesses in the cosmic ray spectrum [6, 7], the GeV excess in the Galactic center as well as a few dwarf spherical galaxies [8] and the possible $\gamma$-ray line in the directions of some galaxy clusters [9]. Nevertheless, further high-quality data are still needed to reliably identify the dark matter annihilation/decay signal. As a part of the international effort to probe dark matter, at the end of 2015 the DArk Matter Particle Explorer (DAMPE) was successfully launched. DAMPE is characterized by its high energy resolution ($\sim 1.5\%$ at 800 GeV) as well as its wide energy range (5 GeV−10 TeV).

The detector of DAMPE consists of 4 sub-detectors [10]. (1) The plastic scintillator detector (PSD) consists of two orthogonal layers ($x$ and $y$ each) of plastic scintillator strips and is designed to distinguish the species of incident heavy ion and to observe non-charged particles (such as photons) and high-energy charged particles (such as electrons). (2) The silicon tracker (STK) is composed of six orthogonal layers ($x$ and $y$ each) of silicon micro-strip detectors, with tungsten plates inserted inside layers 2, 3 and 4, and is developed to measure the incident tracks of high-energy cosmic rays and to identify electrons and gamma rays. (3) The BGO calorimeter can precisely measure the cosmic ray energy and effectively distinguish between electrons and protons. (4) The neutron detector (NUD) can further distinguish between electrons and protons.

In this work we focus on the BGO calorimeter and in

Received 16 April 2016, Revised 3 June 2016

∗ Supported by National Natural Science Foundation of China (11203090, 11003051, 11273070) and Strategic Priority Research Program on Space Science of Chinese Academy of Sciences (XDA04040202)

1) E-mail: huyiming@pmo.ac.cn

particular the results of its environmental test.

## 2 The BGO calorimeter

The BGO calorimeter, shown in Fig. 1, with a size of 907.5 mm×907.5 mm×494.5 mm and a weight of 1051.4 kg, is one of the most important sub-detectors of DAMPE. It is used to measure the spectra of incident high-energy cosmic rays from 5 GeV to 10 TeV and to identify protons and electrons. The BGO calorimeter provides an important background discriminator by measuring the energy deposition due to the particle shower as well as the shower development profile.

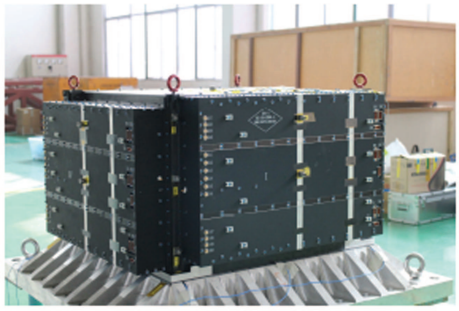

Fig. 1. The BGO calorimeter of DAMPE.

### 2.1 BGO crystal array

The BGO calorimeter is mainly made of 308 bismuth germanate crystals ($Bi_4Ge_3O_{12}$) with a total weight of $\sim$830 kg, accounting for about 78.9% of the whole sub-detector. Each BGO crystal has a size of 25 mm×25 mm×600 mm. All 308 BGO crystals are arranged in 14 layers (about 32 radiation lengths), each composed of 22 crystals coupled with photomultiplier tubes (PMT). Adjacent layers of BGO crystals are orthogonal to each other with $x/y$ orientation respectively. The gaps between neighboring BGO crystals are 4 mm in the vertical direction and 2.5 mm in the horizontal direction.

### 2.2 BGO package structure

The most important purpose of mechanical design is to pack the 308 fragile BGO crystals into one compact sub-detector to form a crystal array, and to ensure the safety and reliability of the BGO calorimeter. It is therefore crucial for the development of the whole detector. During the satellite launch and transition, the structure of the detector should be stable against environmental vibration to ensure the calorimeter operation in normal. An additional requirement for the BGO calorimeter structural design is that metal materials, especially those of high density, could not be used in its detection direction.

Thus, we designed the CFRP (Carbon Fiber Reinforced Plastic) honeycomb case, shown in Fig. 2 as the main supporting structure to pack the crystals. The envelope size is 742 mm×742 mm×494.5 mm. The CFRP honeycomb case is made up of two components. The main part is composed of 308 CFRP square pipes with dimensions of 26 mm×26 mm×700 mm, arranged in 14 pairwise orthogonal layers, the same as the arrangement for the BGO crystals. The other CFRP pipes, consisting of 24 CFRP crossbars and 4 CFRP strut supports, are the load transferring path and the supporting structure of the calorimeter. They are arranged around the main part of the case. The two components are glued together as one whole structure with AG80 to provide not only the space for the BGO crystals, but also the load-bearing structure for the calorimeter. Meanwhile, the CFRP crossbars are imbedded with aluminum inserts to provide threaded holes to fix the PMT protective structures.

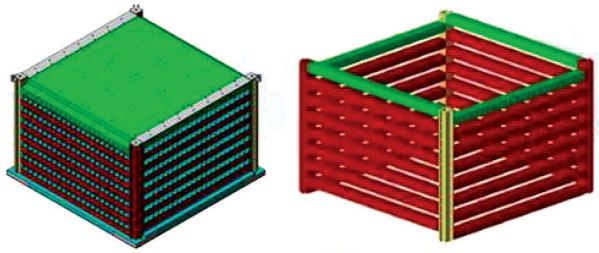

(a) BGO package structure (b) frame of strut supports and crossbars

Fig. 2. The CFRP honeycomb case designed to hold the crystals.

### 2.3 PMT protective structure

The BGO crystals are placed into the square pipes of the CFRP package structure. The 0.5 mm gap between the pipe and crystals is then filled with Dow Corning Sylgard 170 silicone elastomer (DC 170 for short). The square pipe is 100 mm longer than the BGO crystal, which means there is a 50 mm space at each end of the pipe where we can place the PMT to couple with the BGO crystal, with a 50 mm protective structure.

The PMT, covered with 27 μm Permalloy sheet, is placed into the aluminum alloy protective case, filled with DC 170 to seal the PMT inside. On top of the PMT protective unit, the two pre-amplification electronics boards to read out the signal are fixed by the support structure. Then, the whole PMT protective structure is fixed on the crossbars of the BGO package structure. In this way, every BGO crystal and photomultiplier tube with protective structure is arranged entirely inside the CFRP BGO package structure to ensure all important units are in safe condition to resist acceleration and the vibrational load propagation from the rocket during launch.

### 2.4 Overall structure of BGO calorimeter

Besides the CFRP structure, crystals and the PMTs, the overall structure is composed of:

1) An aluminum honeycomb support foundation, within which is imbedded aluminum inserts, constituting the interface of the BGO calorimeter to the satellite baseplate or test fixture;

2) Four aluminum side cases with the Front End Electronic boards that provide EMC shielding and also connectors for power supply and signal;

3) Four aluminum inserts imbedded in the top of the CFRP strut support to provide an interface for the crane.

## 3 Test procedure and realization

### 3.1 Test procedure

The purpose of environmental testing is to simulate the vibration environment and environmental effects during space flight to identify the environmental adaptability of the BGO calorimeter. The tests applied were as follows.

1) Sinusoidal and Random Vibration Test

Sinusoidal vibration and random vibration tests with different levels are determined according to the DAMPE Environmental Test Requirements for Payload and the User Manual for LM-2D. Along each of three mutually perpendicular axes, the BGO calorimeter should pass the random vibration test for 60 seconds each. Also, at the payload level, the BGO calorimeter should pass the sinusoidal vibration test to show its ability to survive the low frequency environment during the satellite launch. The sinusoidal vibration test levels for the BGO calorimeter are listed in Table 1.

2) Modal Surveys

Before and after each run of vibration tests, modal surveys are performed to prove the structure works well by comparing the naturally determined fundamental frequency of the BGO calorimeter appropriately. Each scan runs from 10 to 150 Hz for the horizontal directions ($x/y$ axis), and 300 Hz for the vertical direction ($z$ axis) with integrated amplitude 0.1 g RMS. Here a modal survey is helpful to find out indirectly whether the structure is damaged during the vibration tests, as well as measuring the structural response. If the modal frequency of the BGO calorimeter changes by more than 5%, vibration tests should be stopped and a mechanical check should be performed immediately.

3) Cosmic-ray test

A cosmic-ray test is performed for 120 minutes before random vibration and sinusoidal sweep vibration and at the end of the vibration test. During the cosmic-ray test, basic parameters of the BGO calorimeter including the pedestal and minimum ionizing particles (MIP) response are recorded. The pedestal is the reference voltage level at the signal input front end of the electronic chains. The fluctuation of the pedestal is a generalized Gaussian distribution. The MIP responses are usually calibrated by using cosmic muons at ground level. So the cosmic-ray test is performed to study the basic performance of the BGO calorimeter during the vibration tests. We can tell whether the instrument is in good condition by comparing the change of the basic parameters.

All those tests mentioned above are performed in the sequence shown in Fig. 3.

Table 1. Sinusoidal vibration test level for BGO calorimeter.

| no | axis | frequency/Hz | level ($G_{\rm PEAK}$) |
|---|---|---|---|
| 1 | | 5–8 | 3.88 mm |
| 2 | | 8–40 | 1.0 |
| 3 | $x, y$ | 40–46 | 1.5 |
| 4 | | 46–62 | 2.8 |
| 5 | | 62–90 | 1.0 |
| 6 | | 90–100 | 0.5 |
| no | axis | frequency/Hz | level ($G_{\rm PEAK}$) |
| 1 | | 5–8 | 3.88 mm |
| 2 | | 8–60 | 1.0 |
| 3 | | 60–61 | transition |
| 4 | $z$ | 61–73 | 2.5 |
| 5 | | 73–78 | transition |
| 6 | | 78–85 | 6.0 |
| 7 | | 85–93 | transition |
| 8 | | 93–100 | 2.0 |
| sweep rate | | 2 oct/min | |

### 3.2 Test implementation

The vibration tests were performed at the GuangBo Mechanics Environment Laboratory in Suzhou, China, with a DC-30000-300/SC2020 electro-dynamic vibration test system.

During the test, an aluminum test fixture with dimensions 1200 mm×1200 mm×150 mm was designed to fix the BGO calorimeter. As shown in Fig. 4, the fixture provided the interface not only to the vibration test system, but also to the BGO calorimeter. Holes and slots were machined on the fixture to mount the accelerometers easily. Five accelerations were put inside the fixture to provide the control signal during the vibration tests.

The instrument was composed of 5 control tri-axial accelerometers and 21 tri-axial accelerometers attached to the BGO calorimeter for surveying during the test. The accelerometers were located as follows: each CFRP strut support contained three accelerometers (upper and lower three parts), each aluminum side case contained two accelerometers (upper and middle part), and the last one was attached on the middle of the top of the BGO calorimeter.

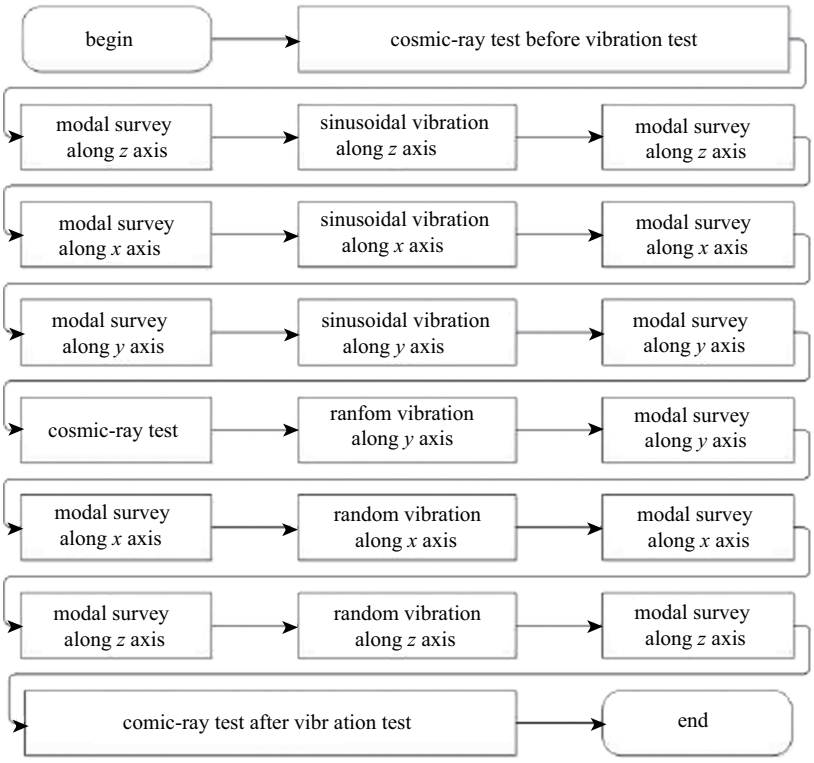


Fig. 3. Sequence of the BGO calorimeter enviromental tests.

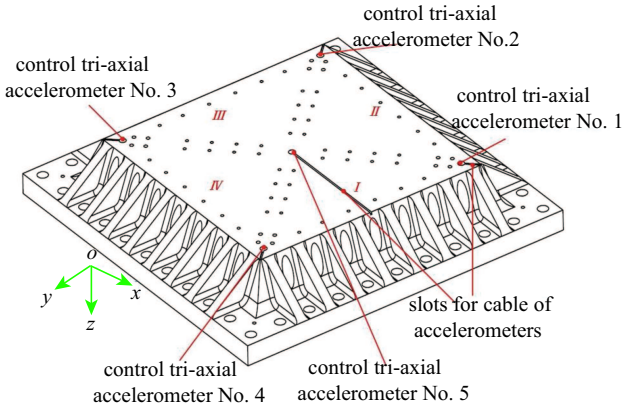


Fig. 4. Five accelerations were put inside the fixture to provide the control signal during the vibration tests.

## 4 Test results

### 4.1 Sinusoidal vibration and random vibration

Sinusoidal vibration tests were applied to all axes with the levels shown above. The maximum acceleration measured by the accelerometers was 6.66 g at the $-y$ side aluminum side-case. Pre-test and post-test inspections were performed of the main supporting structure, the Faraday aluminum case in each direction, showing that no damage occurred during the vibration test of the BGO calorimeter. The screws were well fastened, displacements were very small and agreed with the predictions. The calorimeter is expected to survive the static equivalent launch environment without damage during the sinusoidal vibration.

Random vibration tests were performed in all three directions with an identical input level of 4.45 g RMS for each. According to the GSFC-STD-7000 standard [11], due to the weight of the BGO calorimeter being greater than 182 kg, the plateau acceleration spectral density level (ASD) was reduced to 0.01 $g^2$/Hz from 20 to 2000 Hz with an overall level of 4.45 g RMS. One of the purposes of the random vibration test is to determine the response of the CFRP supporting structure and FEE boards to ensure no damage occurs during launch. The results of the random vibration are summarized in Table 2. The measured values are well below the currently adopted stay-clear limits and agree with the predicted values.

### 4.2 Modal surveys

Any significant change in modal characteristics, frequency and modal shape of vibration directly provides an indication of structural damage [12]. Modal surveys were applied on each axis to detect the change of natural frequency of the BGO calorimeter. For the $x$-axis and

$y$-axis, the modal survey scan ran from 10 to 150 Hz, and the first natural frequency of the BGO calorimeter was found between 115 and 125 Hz from the responses of those accelerometers. For the $z$-axis, the scan range extended to 300 Hz, and the first natural frequency was found between 220 and 230 Hz. One of the amplitude results measured by the accelerometer located at the side case are shown in Fig. 5. All four curves are superposed and show no obvious change during the tests. According to the results of the vibration tests, changes of the first natural frequency of the BGO calorimeter are less than 5%, of which the largest change is 3.29%. After random or sinusoidal vibrations, there is no obvious variation of the frequency signatures observed.

Table 2. Results of the BGO calorimeter during the random vibration. ("A" is short for "Acceleration".)

| position | vibration along $x$ | | vibration along $y$ | | vibration along $z$ | |
|---|---|---|---|---|---|---|
| | A.(g, RMS) | D.(mm, RMS) | A.(g, RMS) | D.(mm, RMS) | A.(g, RMS) | D.(mm, RMS) |
| aluminum side case($+x$ side upper part) | 10.03 | 0.21 | 6.86 | 0.22 | 9.21 | 0.18 |
| aluminum side case($-y$ side upper part) | 6.06 | 0.20 | 8.14 | 0.22 | 9.00 | 0.20 |
| aluminum side case($-x$ side upper part) | 7.52 | 0.21 | 6.76 | 0.21 | 8.96 | 0.17 |
| aluminum side case($+y$ side upper part) | 5.97 | 0.20 | 7.03 | 0.21 | 7.45 | 0.17 |
| aluminum side case($+x$ side middle part) | 16.75 | 0.20 | 3.48 | 0.20 | 8.86 | 0.17 |
| aluminum side case($-y$ side middle part) | 5.79 | 0.19 | 24.35 | 0.20 | 8.10 | 0.18 |
| aluminum side case($-x$ side middle part) | 17.06 | 0.20 | 5.72 | 0.20 | 8.80 | 0.17 |
| aluminum side case($+y$ side middle part) | 5.70 | 0.19 | 25.57 | 0.20 | 7.27 | 0.17 |
| strut support($+x,-y$ side upper part) | 4.86 | 0.21 | 5.28 | 0.21 | 4.40 | 0.18 |
| strut support($-y,-x$ side upper part) | 5.10 | 0.21 | 5.56 | 0.21 | 4.40 | 0.17 |
| strut support($-x,+y$ side upper part) | 4.79 | 0.21 | 5.57 | 0.21 | 3.99 | 0.17 |
| strut support($+x,+y$ side upper part) | 5.16 | 0.21 | 5.34 | 0.21 | 4.49 | 0.18 |
| strut support($+x,-y$ side middle part) | 3.49 | 0.19 | 3.68 | 0.20 | 3.84 | 0.17 |
| strut support($-y,-x$ side middle part) | 3.39 | 0.20 | 3.87 | 0.20 | 3.85 | 0.17 |
| strut support($-x,+y$ side middle part) | 3.35 | 0.19 | 3.76 | 0.20 | 3.52 | 0.17 |
| strut support($+x,+y$ side middle part) | 3.27 | 0.19 | 3.61 | 0.20 | 3.94 | 0.18 |
| strut support($+x,-y$ side lower part) | 3.01 | 0.18 | 3.00 | 0.18 | 3.29 | 0.18 |
| strut support($-y,-x$ side lower part) | 3.32 | 0.19 | 3.83 | 0.19 | 3.49 | 0.17 |
| strut support($-x,+y$ side lower part) | 3.41 | 0.18 | 3.47 | 0.18 | 3.61 | 0.17 |
| strut support($+x,+y$ side lower part) | 3.07 | 0.18 | 3.54 | 0.18 | 3.52 | 0.18 |
| center point on the top | 6.09 | 0.21 | 6.54 | 0.22 | 11.51 | 0.18 |

### 4.3 Cosmic-ray test

Before and after the environmental tests, cosmic-ray tests were applied and the results are shown in Table 3, where we can find that there is no obvious change in either the MIP responses or the pedestals of sensitive detector output of the first layer of the calorimeter in the +x side during the cosmic-ray tests. Figure 6 shows the shift ratio of Most Probable Value (MPV) of MIPs changes before and after the environmental tests. The mean value of the shift ratio is about $-4\%$. The MPV after the vibration test is a little lower than before. In Fig. 7 and Fig. 8, the results of pedestals of all channels are shown, and in Fig. 9, we can find the MIP peak positions of every BGO crystal. These results show that no measurable damage occurred during the vibration and the performance of the calorimeter is stable.

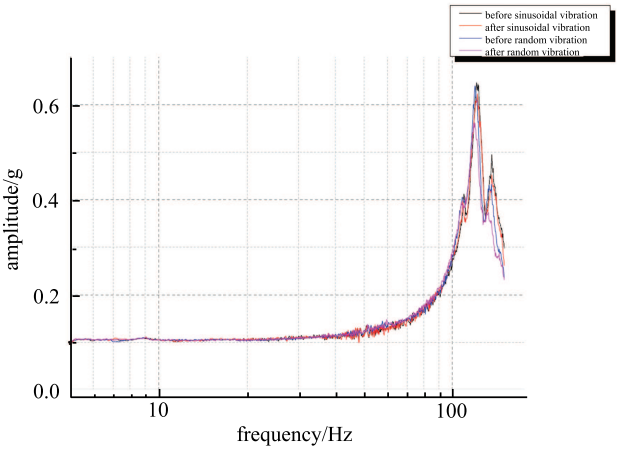


Fig. 5. Amplitude before and after vibration measured by the accelerometer at the side case.

Furthermore, only one bar's MPV shift ratio, for a bar at the edge of the calorimeter (layer 8, BGO ID 22), is close to 20%. This difference is also shown in the 3rd picture of left column of Fig. 9. The reason may be that the degree of coupling between the BGO crystal and the PMT used to collect the scintillation light was changed. During the development of the BGO calorimeter, an optical rubber with attenuation filter was inserted into the gap between each BGO crystal and PMT. The stress of the optical rubber may be released during the vibration. We focused on this channel in the following tests and found the MIP signal was very stable.

Table 3. There is no obvious change in either the MIP responses or the pedestals of sensitive detector output of the first layer of the calorimeter in the $+x$ side during the cosmic-ray tests.

| BGO ID | pedestal position | | pedestal sigma | | MIPs | |
|---|---|---|---|---|---|---|
| | before test | after test | before test | after test | before test | after test |
| 1 | 155.4 | 154.9 | 8.2 | 8.2 | 481.1 | 453.6 |
| 2 | 161.1 | 159.9 | 8.5 | 8.4 | 507.9 | 513.4 |
| 3 | 170.8 | 169.8 | 8.4 | 8.4 | 492.5 | 490.6 |
| 4 | 117.4 | 116.7 | 8.4 | 8.4 | 445.5 | 433.9 |
| 5 | 115.4 | 114.5 | 8.3 | 8.3 | 405.8 | 389.1 |
| 6 | 115.9 | 114.9 | 8.0 | 7.9 | 484.9 | 470.3 |
| 7 | 112.6 | 111.6 | 8.0 | 8.0 | 497.8 | 486.3 |
| 8 | 97.5 | 96.7 | 7.8 | 7.7 | 489.5 | 485.3 |
| 9 | 112.3 | 111.1 | 7.9 | 7.8 | 444.0 | 460.8 |
| 10 | 119.1 | 117.8 | 7.7 | 7.7 | 452.8 | 467.8 |
| 11 | 17.0 | 16.7 | 7.5 | 7.5 | 412.2 | 395.4 |
| 12 | 105.7 | 104.9 | 7.6 | 7.6 | 416.0 | 392.7 |
| 13 | 93.1 | 92.7 | 7.4 | 7.4 | 430.1 | 442.1 |
| 14 | 59.1 | 58.5 | 7.6 | 7.6 | 378.6 | 372.1 |
| 15 | −17.9 | −18.0 | 7.9 | 7.9 | 460.2 | 462.4 |
| 16 | −20.1 | −20.6 | 7.6 | 7.6 | 363.2 | 363.8 |
| 17 | 20.6 | 20.3 | 7.6 | 7.6 | 455.5 | 475.8 |
| 18 | 32.8 | 32.6 | 8.0 | 8.0 | 574.2 | 548.5 |
| 19 | −34.0 | −33.9 | 7.9 | 7.9 | 467.3 | 478 |
| 20 | 48.4 | 48.2 | 8.0 | 8.0 | 400.6 | 384.2 |
| 21 | −48.0 | −48.0 | 8.3 | 8.2 | 468.5 | 460.6 |
| 22 | −36.1 | −36.1 | 8.3 | 8.2 | 560.0 | 557.0 |

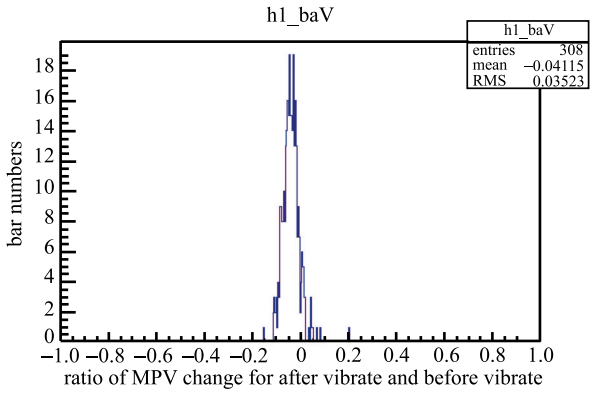


Fig. 6. The shift ratio of most probable value of MIPs changes.

## 5 Conclusions

Displacements during random vibrations as well as sinusoidal vibrations are found to be well below the stay-clear conditions. The results of the inspection and modal surveys confirm that no damage occurred during the testing of the calorimeter. MIP peak positions and pedestals of every channel were recorded. The results show that the shift ratio of the MPV of MIPS is about −4%. The results of the cosmic-ray tests confirm that the performance of calorimeter is in good condition and no damage was caused to the sensitive detectors (crystals and PMTs). All these results suggest that the calorimeter and its structure have passed through the environmental tests successfully.

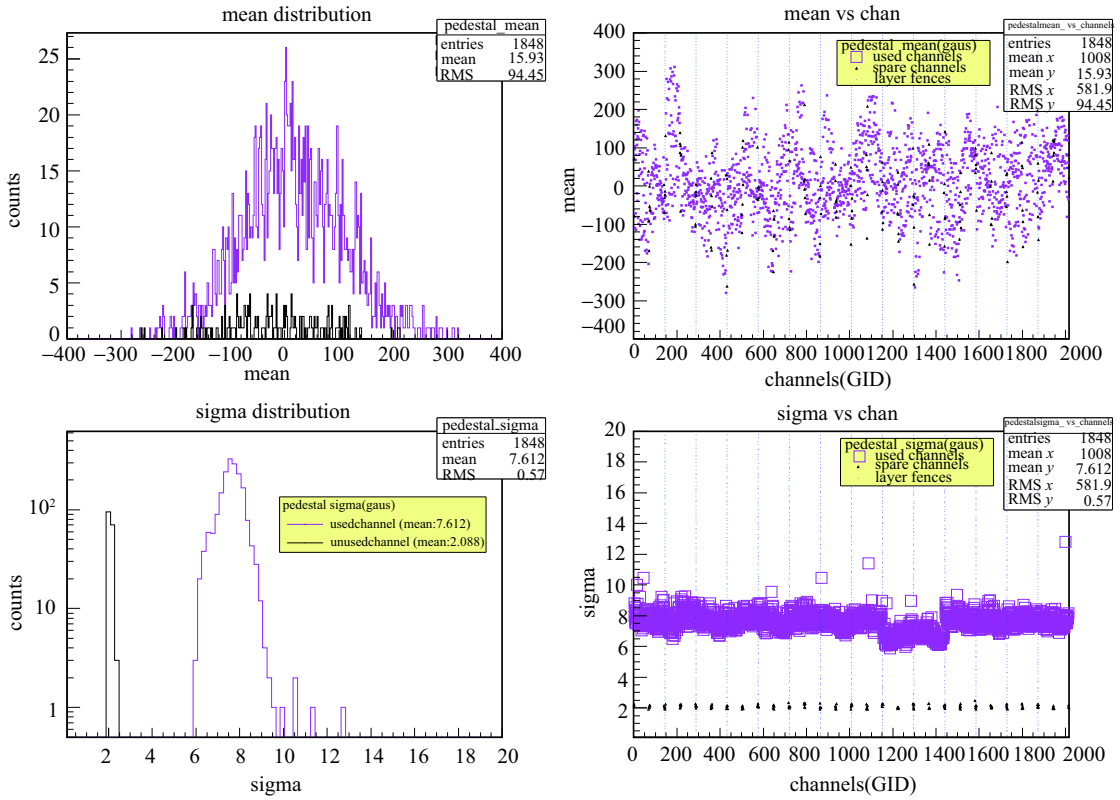


Fig. 7. The results of pedestal signals of every channel before vibration.

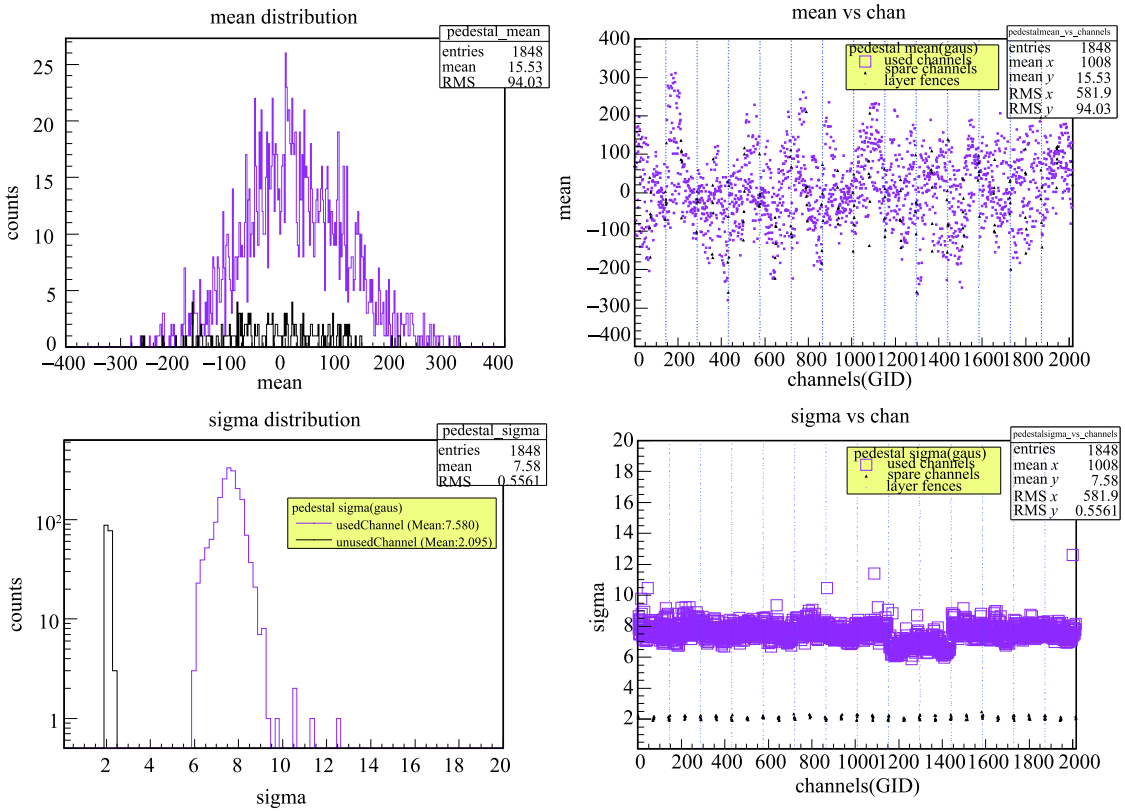


Fig. 8. The results of pedestal signals of every channel after vibration.

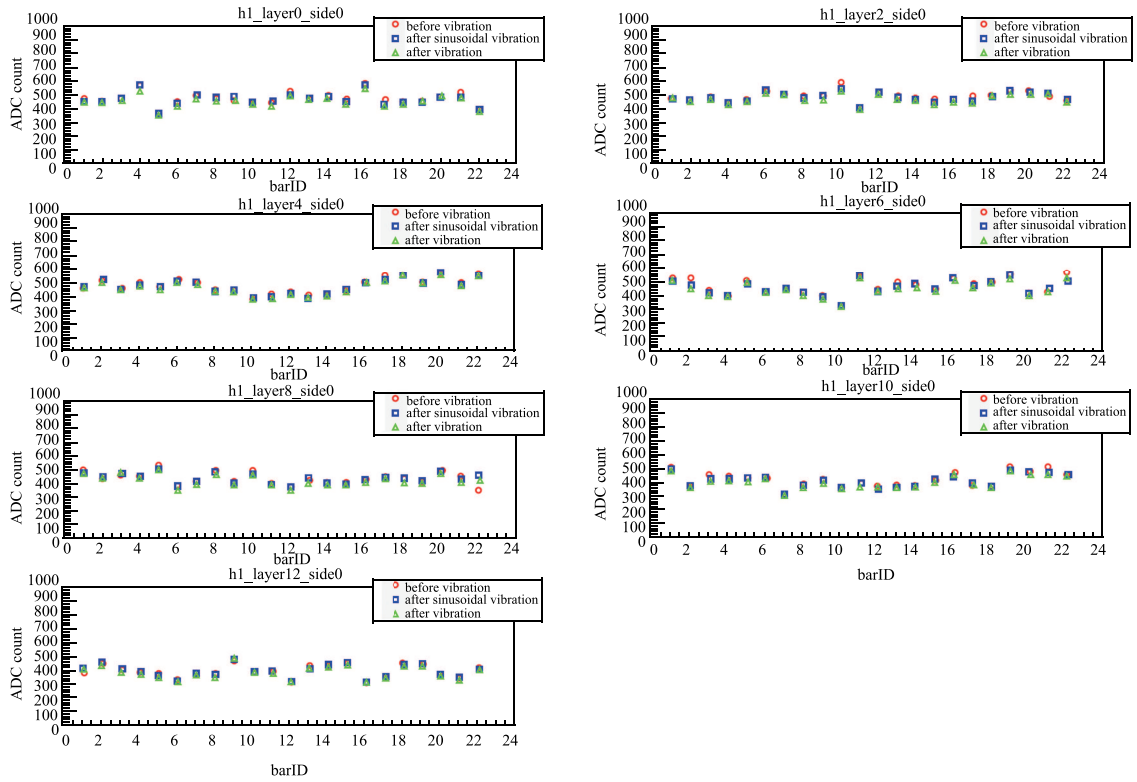


Fig. 9. The MIP peak positions of every BGO crystal on the $+x$ side.

## References


1 G. Bertone, D. Hooper, J. Silk et al, Physics Reports, **405**: 279–390 (2005)
2 J. L. Feng, Ann. Rev. Astron. Astrophys., **48**: 495–545 (2010)
3 Y. Z. Fan, B. Zhang, and J. Chang, IJMPD, **19**: 2011–2058 (2010)
4 P. Picozza, R. Sparvoli, NIMPA, **623**: 672–676 (2010)
5 W.B. Atwood, A. A. Abdo, M. Ackermann et al, The Astrophysical Journal, **697**: 1071–1102 (2009)
6 M. Aguilar, G. Alberti, B. Alpat et al, Phys. Rev. Lett., **110**: ID–141102 (2013)
7 J. Chang, J. H. Adams, S. H. Ahn et al, Nature, **456**: 362–365 (2008)
8 S. Li, Y. F. Liang, K. K. Duan et al, Phys. Rev. D, **93**: ID–043518 (2016)
9 Y. F. Liang, S. Q. Shen, X. Li et al, astro-ph.HE arXiv:1602.06527 (2016)
10 J. Chang, Chinese Journal of Space Science, **34**: 550–557 (2014)
11 NASA GODDARD SPACE FLIGHT CENTER, 2005, GSFC-STD-7000
12 O. Ferreira, G. Bogaert, A. Bonnemaison et al, NIMPA, **530**: 323–329 (2004)